Published in final edited form as:
Magn Reson Med. 2013 May ; 69(5): 1357–1366. doi:10.1002/mrm.24379.

CONTRIBUTIONS OF CHEMICAL AND DIFFUSIVE EXCHANGE TO $T_{1\rho}$ DISPERSION

Jared Guthrie Cobb, PhD[1,2], **Jingping Xie, PhD**[2], and **John C. Gore, PhD**[1,2,3]

[1]Vanderbilt University Department of Biomedical Engineering

[2]Vanderbilt University Institute of Imaging Science

[3]Vanderbilt University Department of Radiology and Radiological Sciences

Abstract

Variations in local magnetic susceptibility may induce magnetic field gradients that affect the signals acquired for MR imaging. Under appropriate diffusion conditions, such fields produce effects similar to slow chemical exchange. These effects may also be found in combination with other chemical exchange processes at multiple time scales. We investigate these effects with simulations and measurements to determine their contributions to rotating frame ($R_{1\rho}$) relaxation in model systems.

Simulations of diffusive and chemical exchange effects on $R_{1\rho}$ dispersion were performed using the Bloch equations. Additionally, $R_{1\rho}$ dispersion was measured in suspensions of Sephadex and latex beads with varying spin locking fields at 9.4T. A novel analysis method was used to iteratively fit for apparent chemical and diffusive exchange rates with a model by Chopra et al.

Single- and double-inflection points in $R_{1\rho}$ dispersion profiles were observed, respectively, in simulations of slow diffusive exchange alone and when combined with rapid chemical exchange. These simulations were consistent with measurements of $R_{1\rho}$ in latex bead suspensions and small-diameter Sephadex beads that showed single- and double-inflection points, respectively. These observations, along with measurements following changes in temperature and pH, are consistent with the combined effects of slow diffusion and rapid $^{-}$OH exchange processes.

Keywords

T1rho; dispersion; diffusion; chemical exchange

INTRODUCTION

Within a heterogeneous medium, variations in the local magnetic susceptibility may induce gradients in magnetic field that affect the signals acquired for MR imaging. The decay of transverse magnetization is then accelerated, but the precise effects depend on several factors including the sizes of the field perturbations, their spatial extent and geometry, the rate of spin diffusion in their vicinity, and the pulse sequence. One theoretical description that affords useful insights into how these factors interplay is the Anderson-Weiss Mean Field approach previously applied to transverse relaxation in MRI by Kennan et al. (1). Spin-lattice relaxation in the rotating frame with rate $R_{1\rho}$ is also sensitive to variations in the local magnetic field experienced by nuclei that vary on the time scale of an applied radiofrequency spin-locking field that is under experimental control. Values of $R_{1\rho}$

Jared Cobb, VUIIS, AA 3112 MCN, 1161 21st Ave South, Nashville, TN 37232-2310. 615-356-1156, jared.g.cobb@vanderbilt.edu.

generally decrease from R_2 to R_1 as the locking field increases, and the dispersion reflects the characteristic time scale of irreversible dephasing effects (2). In principle, measurements of $R_{1\rho}$ dispersion may be used to estimate some intrinsic properties of the medium. For example, in biological media, if the intrinsic diffusion coefficient D is of order 2×10^{-5} cm^2s^{-1}, the time required to move 2 μm is 1 msec. If variations of field are present on this spatial scale we may expect to observe significant $R_{1\rho}$ dispersion around locking fields of 1 kHz, well within the regime readily accessible in practical MRI experiments. When the scale is much larger, dispersion will occur at correspondingly lower frequencies. Potentially, therefore diffusion dephasing within a magnetically inhomogeneous medium may contribute to $R_{1\rho}$ dispersion measurements, and appear similar to a chemical exchange process.

A second major potential contributor to $R_{1\rho}$ dispersion is more rapid chemical exchange between water protons and labile groups in solute molecules. This dispersion depends, amongst other factors, on the exchange rate and the chemical shift of the exchanging species. In biological samples, $R_{1\rho}$ dispersion may be typically dominated by the chemical exchange of hydroxyl, amine, and / or amide protons. In a medium containing variations in bulk susceptibility and chemically exchanging protons, the $R_{1\rho}$ dispersion will reflect the integrated effects of both diffusion and chemical exchange. Here we consider some simple systems that demonstrate these behaviors and show how these different mechanisms may be separately identified. By using an appropriate theory and analysis, useful parameters that describe the samples may be quantified.

A precise description of diffusion through gradients requires a computation of the continuous dephasing that occurs over time due to random motions. We recently derived an analytical expression for the contribution to $R_{1\rho}$ from diffusion through gradients with a characteristic spatial frequency (Gore, Submitted to J. Magn. Res., 2012). However, here we show how in practice we can use the approximation that diffusion may be represented as slow exchange between regions of discrete frequencies, which simplifies the analysis considerably.

Intrinsic field gradients in tissues caused by variations in bulk magnetic susceptibility ($\Delta\chi$) have a spatial scale that reflects the size of the inhomogeneity. For example, micron-scale effects may arise around deposits of iron or calcium or because of the influence of microvascular changes in blood oxygenation, the basis of the blood level oxygen dependence (BOLD) effect on R_2* (1). Diffusion around such inhomogeneities causes dephasing and effective relaxation. The distance scale over which the local field varies significantly depends on the size of the inhomogeneity while the gradient amplitude depends on the difference in $\Delta\chi$.

Here we consider the $R_{1\rho}$ dispersion characteristics of water in the presence of packed arrays of small spherical beads. Latex beads represent the situation where the field is disturbed by the susceptibility mismatch between latex and water with no other proton pools extant. Sephadex® beads consist of cross-linked dextran sugars that swell when hydrated and are a useful model system to explore the combined effects of susceptibility, diffusion, and chemical exchange (3,4). They are commercially available in a variety of sizes and cross-link densities. The beads are permeable to the extent that water may freely diffuse between the inner dextran and outside water pools. Quantitative measurements of these effects have previously been made with Carr-Purcell-Meiboom-Gill (CPMG) techniques and result in enhanced transverse relaxation at a rate proportional to the pulse spacing (1,4,5).

Proton relaxation inside Sephadex beads is dominated by hydroxyl ($^-$OH) chemical exchange as reported by Hills et al. (4,6). However, Hills et al. noted that under certain experimental conditions, diffusive exchange behaves like slow chemical exchange and a

double-dispersion is observable in CPMG experiments in which the pulse rate is varied (6,7). Hills proposed a model that attributes the observed low frequency dispersion to a combination of diffusive exchange from within the beads to the solvent and diffusion through the susceptibility gradients exterior to the beads. The simplified diffusive exchange model is characterized by protons moving between two spatially uniform parts of a sample (e.g. between water and Sephadex bead) where their spins experience different relaxation rates or are imparted with a different resonant frequency as shown in Figure 1. The characteristic rate for diffusive exchange is expected to be ~D/r^2, where 'D' is the diffusion coefficient and 'r' is the mean bead radius (4). The same time scale is relevant for the case of diffusion among susceptibility gradients external to the beads, as is the case for latex.

While Hills and others have measured CPMG dispersions, it is often technically easier to measure a greater range of spin lock frequencies than equivalent CPMG pulse rates. Therefore, dispersive effects due to exchange may be apparent over a wider range of locking fields as compared to CPMG dispersion. We demonstrate that slow diffusive exchange may be approximated as slow chemical exchange with simulations of the Bloch-McConnell equations (as opposed to the traditionally used Bloch-Torrey equations governing diffusion). To fit simulated and experimental $R_{1\rho}$ data to a model that contains both diffusive and chemical exchange, we propose extending the model of chemical exchange under spin-locking conditions by Chopra et al. to fit a double-dispersion curve (8). We show how this fits the simulated data and evaluate its suitability for estimating chemical and diffusive exchange rates in experiments on relevant model samples. Spin lock dispersion measurements may potentially technique may be refined to quantify particle size or bulk magnetic susceptibility in tissues with altered chemical exchange and diffusion relaxation processes such as iron deposits and lesion associated with multiple sclerosis or Alzheimer's Disease. Haacke, Zhang, and Hills have quantified such features with alternate MR methods (9–11).

THEORY

Dispersion data in porous beads containing labile protons are characterized by three dynamic processes, of which two depend on the resonant frequency difference between the inside of the bead and the exterior solvent. If this frequency difference is larger than the inverse of the time required to sample each spatial domain this corresponds to a "fast" diffusion regime and the net result is conceptually similar to chemical exchange between phases with rate ~D/r^2 (6,12). When the rate of diffusion is much slower and the exchange rate is less than the frequency difference, nuclei do not sample all spatial areas. This results in different degrees of dephasing and more complex multi-exponential relaxation (6).

A second diffusion-related process is water diffusion through locally induced field gradients caused by susceptibility differences (1). For sphere-shaped objects, the gradients occur externally to the particles, and Eq. 1 gives the average field gradient generated,

$$G=\mu_0 B_0 \Delta\chi/(4r) \quad [1]$$

where μ_0 is the magnetic permeability of free space, B_0 is the main field strength, $\Delta\chi$ is the magnetic susceptibility difference between substances, and 'r' is the object radius (13). For transverse relaxation, this mechanism contributes an additional diffusion-related term shown in Eq 2.

$$R_{2,obs}=R_2+D(\gamma G\tau)^2/3 \quad [2]$$

where R_2 is the intrinsic spin-spin relaxation rate, D is the diffusion coefficient, γ is the gyromagnetic ratio, G is the induced field gradient, and τ is the interval between refocusing

pulses in a CPMG measurement that defines the time scale for irreversible spin dephasing. For rotating frame relaxation we can conceptually identify τ with the period of the locking pulse $(\gamma B_1)^{-1}$. Gore (Submitted to J. Magn. Res., 2012) has analyzed the effects of diffusion in a sinusoidal gradient of spatial frequency q and amplitude g, giving Equations 3 and 4.

$$R_{1\rho,\mathrm{obs}} = R^0_{1\rho} + \frac{\gamma^2 g^2 D}{(q^2 D)^2 + \omega_1^2} \quad [3]$$

$$= R^0_{1\rho} + \gamma^2 g^2 D \times \frac{\tau_c^2}{1 + \omega_1^2 \tau_c^2} \quad [4]$$

where $\tau_c = (Dq^2)^{-1}$, $R_{1\rho,\mathrm{obs}}$ is the observed rotating frame relaxation rate, R^0_{1c} is the rotating frame relaxation rate when $\frac{\gamma B_1}{2\pi}$ approaches 0 Hz (8), and $\omega_1 = \gamma B_1$ is the applied locking field strength. For close packed spheres, we can approximate q as being $\sim\pi/r$. Hills et al. attribute a midpoint of a region of dispersion to the relevant mean diffusive or chemical exchange rate (6). There, $1/\tau_c = Dq^2$ corresponds to the appropriate rate. However, if other parameters such as the relaxivities and chemical shifts of the exchanging species are known, Chopra, Hills, Woessner and others have shown that more precise estimates of chemical exchange may be fitted from rotating frame or CPMG dispersion data (3,8,14).

METHODS

Simulations of Diffusive and Chemical Exchange Effects on $R_{1\rho}$

In order to evaluate potential contributions of chemical and diffusive exchange to $R_{1\rho}$ measurements, simulations were performed using reference values for dextran and Sephadex bead (3,15) in combination with the Bloch equations modified for chemical exchange in a manner described by Hills with minor corrections for consistency of notation (16). We model the system as three pools of protons. Pool A represents the free water outside the beads that experience the external field gradients. Pool B is the rapidly exchanging hydroxyl sites on the surface and interior of the dextran bead, and pool C represents those water molecules that diffuse from the inside to the outside of the beads and experience a shift in field and resonance frequency as shown in Figure 1. The equations governing the simulations have been published previously by several authors (17,18), and are listed in the Appendix. Note that both Pools A and C experience field perturbations with the time scale $\sim r^2/D$ and will appear like water in relatively slow exchange.

Simulated data were generated to illustrate the effects of increasing the mean diffusive exchange rate or the scale of the local magnetic field gradients (k_{ca}) and to separately scale the mean chemical exchange rate (k_{ba}) to generate double-dispersion relaxation profiles. The chemical exchange rate was increased from 1 to 10 kHz while keeping the diffusive rate equal to 5 Hz. This rate is in the typical range for rapid hydroxyl exchange in sugar solutions (19). The diffusive exchange rate (k_{ca}) was increased from 5 to 50 Hz, which is consistent with other observations of such rates (3), with an accompanying chemical exchange rate that is well separated at 10 kHz to simulate the effect of decreasing the spatial dimensions of intrinsic gradients. The data were simulated at main fields of $\omega_0 = 2\pi$*(200 and 400) MHz over a range of locking fields (ω_1) achievable experimentally from 2π*[1 Hz to 10 kHz]. The remaining model characteristics were kept constant at $T_{1a} = 3$ sec, $T_{2a} = 2$ sec, $T_{1b} = T_{1c} = 1$ sec, $T_{2b} = T_{2c} = 30$ msec, $p_a = 0.99$, $p_b = p_c = 0.005$, $\Delta\omega_{ba} = 1.23$ ppm, $\Delta\omega_{ca} = 1.23$ ppm or 0.123 ppm. Two values of $\Delta\omega_{ca}$ were used in simulation to model a range of systems whose slow diffusive exchange component (Pool C to A) is dominated by either a

~1 ppm frequency shift that is typical of a hydroxyl resonance or is dominated by a susceptibility-induced field that is typically an order of magnitude less for latex or ~0.1 ppm. Additionally, T_{2b} times are expected to change with bead density, and the values used here are approximate for G100-50 and were taken from fitted CPMG dispersion experiments by Hills et al. (3).

To more closely approximate experimental measurements, zero-mean Gaussian white noise was added to the simulated double-dispersion relaxation data, and the noisy data were subsequently fit to the double dispersion model of chemical and diffusive exchange described in the data analysis section below using a Levenberg-Marquardt based non-linear least squares fitting algorithm implemented in MATLAB (R2010a, MATLAB, Natick, MA).

Materials

Samples of Sephadex® were obtained from Sigma-Aldrich in the following sizes and densities: G100-50, G100–120, G25–300, and G25–50. For a given product label GX-Y, X represents mean density and Y represents mean radius in microns (μm). The density is expressed as a percent weight of dextran equal to 1000/X. Fore example, a product label of G100-50 would contain beads of density X = 100 with mean radius Y = 50 μm. Thus, the concentration of dextran inside a G100-50 bead is much lower (~10 % wt/wt) than in a G25–50 bead (~40%), which affects relaxation times of water within the beads. Phantoms of close packed, fully saturated beads were prepared by addition of distilled and deionized Milipore® water to a known dry weight of Sephadex beads. The bead and water mixtures were transferred to 5mm NMR tubes, and gently stirred to create an even mixture. The tubes were sealed and allowed to rest for 24 h before being used in any experiment.

Additional samples of G100-50 and G25–50 were prepared over a pH range of 6 to 9 in 1X PBS buffer to selectively accelerate chemical exchange by the addition of HCL or NaOH to the 0.6 mL microtubes. The total amount of liquid was held constant as compared to the unmodified samples.

A similarly sized bead phantom, without interior water or a chemically exchanging species, was created from 47-micron diameter latex beads (07314-5) that were obtained from PolySciences (Warrington, PA) and centrifuged to create a close-packed mixture similar to the Sephadex beads.

NMR Experiments

All NMR experiments were performed on a Varian 9.4T magnet at 400 MHz (Varian Medical Systems, Palo Alto, CA) with a 5- or 10-mm loop-gap coil. Temperature was monitored by thermocouple connected to an animal physiologic monitoring system (SA Instruments, Stony Brook, NY) and was maintained at 25 or 40° C.

$T_{1\rho}$ dispersion was measured with a spin-locking sequence consisting of an adiabatic 90-degree pulse (AHP), followed by an on-resonance spin-locking (SL) pulse for half of the spin lock time (SLT), then a 180 degree refocusing pulse, followed by the other half of the spin lock pulse with reversed phase, and signal readout as described by Sepponen et al. and Witschey et al. (20,21). The SL pulse was varied logarithmically in 10 time increments between 10 msec and 2 sec and also in amplitude (SLA) in 21 increments between 2π*[1 Hz and 10 kHz]. Low SLA and short SLT data were acquired first to minimize any effects of sample heating. The maximum allowed spectral line width with first and second order shims was 35 Hz for G25-Y beads, 25 Hz for G100-Y beads, and 12 Hz for the latex beads. TR was set at 5 times the estimated T_1 for each solution.

Data Analysis

$R_{1\rho}$ values were calculated by fitting the signal variation with SLT to a three-parameter mono-exponential decay function in MATLAB (The MathWorks, Inc., Natick, MA).

$$S(t)=S_0 \exp\left(-t*R_{1\rho}\right)+C \quad [4]$$

We propose fitting double-dispersion data iteratively to the Chopra equation for chemical exchange contribution to $R_{1\rho}$ ($1/T_{1\rho}$) dispersion, shown in Eq. 5 (8)

$$R_{1\rho}=\left\{\frac{R_2+\frac{\left(R_{1\rho}^{\infty}*\omega_1^2\right)}{S_\rho^2}}{1+\frac{\omega_1^2}{S_\rho^2}}\right\} \quad [5]$$

$$\text{where, } S_\rho{}^2=(R_{1b}+k_{ex})/(R_{2b}+k_{ex})*\{(R_{2b}+k_{ex})^2+\Delta\omega_b{}^2\}. \quad [6]$$

A non-linear least squares fit of the variation of $R_{1\rho}$ with ω_1, ($\omega_1 = \gamma B_1$), to Eq. 5 may be used to obtain best fits of R_2, $R_{1\rho}^{\infty}$ ($R_{1\rho}^{\infty}$;R_1), and S_ρ^2, where S_ρ is the midpoint between the R_2 and $R_{1\rho}^{\infty}$ values. For systems where multiple exchange processes are sufficiently separated in frequency we expect distinct double-dispersion profiles in measured $R_{1\rho}$. By taking the second derivative of the double-dispersion data, the three resulting zero crossings are assumed to define the boundaries of the low frequency diffusive exchange regime, the transition point from the diffusion dominated regime to chemical exchange dominated regime, and finally the higher frequency chemical exchange regime of the curve. With the exchange regimes thus separated, the data in the slow exchange regime are fit to Eq. 5, where the slow diffusion exchange rate ($k_{ex} = k_{ca}$) is expected to correspond to a midpoint in the dispersion curve (S_ρ), consistent with the observations of Hills (4). In the fast chemical exchange region the $R_{1\rho}$ values are fit to the full Chopra model (by including Eq. 6) to give the fast exchange component ($k_{ex} = k_{ba}$). The necessary chemical shift and other relaxation parameters are identical to those used in the simulations. This approach to fitting for fast chemical exchange rates has been previously used in cartilage systems and also in poly-acrylamide gels (22,23). By measuring the change in observed $R_{1\rho}$, G_{avg} in the solution can be estimated and then subsequently the mean $\Delta\chi$ using Eqs. 3 and 1 respectively, assuming a spherical geometry.

RESULTS

Simulation Results

Initial simulations of rapid diffusive exchange approximating chemical exchange explored the role of the frequency shift between pools C and A. The frequency ω_{ca} was varied from the chemical shift of dextran, ~1.23 ppm, to a frequency shift an order of magnitude lower, or ~25 Hz at main field strength of 200 MHz, representing a system with only diffusion through susceptibility gradients and no chemical exchange. The results are shown in Fig. 2.a. The larger frequency shift represents a system dominated by diffusive exchange approximating slow chemical exchange and is shown in Figure 2.b. The $R_{1\rho}$ dispersion profile scales with the exchange rate, k_{ca}, with an inflection point near ~250 Hz that corresponds roughly to the sum of the simulated chemical shift and exchange rate.

Simulations of combined chemical and diffusive exchange were performed to create $R_{1\rho}$ double-dispersion profiles across a range of exchange rates, locking fields, and spectrometer frequencies. The effect of increasing the diffusive exchange rate from 5 to 50 Hz at $\omega_0 = 2\pi*200$ MHz, with chemical exchange rate of 10 kHz, is shown in Figure 3.a. Here the double dispersion profile is clearly demonstrated at low SLA, with $R^0_{1\rho}$ increasing from 2.4 to 2.7 s^{-1}. Figure 3.b. shows the effect of increasing chemical exchange rate from 1 kHz to 10 kHz with a constant diffusive exchange rate. This figure shows increased separation between the two exchanging processes.

These simulated data were then used to test the ability of the Chopra expression to fit for the two exchange processes. The results of progressively adding noise to the closely spaced curve (5 Hz diffusive rate, and 1 kHz chemical exchange rate, at 400 MHz main field) are given in Table 1. The fitting for the chemical exchange rate is accurate within 8% of the simulated rate until the signal to noise ratio (SNR) drops below 20:1. The diffusive exchange rate is accurate only within 40% of the simulated rate until the SNR also drops below 20:1, at which point the double-dispersion is lost in noise and the fitting fails.

Sample noisy data fits with SNR = 80:1 with simulated data points, and fitted parameters from the fitting procedure shown in Figure 4. The chemical exchange region is shown with a solid red fit line and the diffusive exchange region is shown with a solid blue line. The second derivative is shown as a dashed black line and illustrates where the zero crossings intersect the fitted data.

Sample fits of the simulated data from Figure 3.a and 3.b are given in Figure 4.b and 4.c respectively. Note that the increase in diffusive rate in Figure 4.b has little effect on the fitted chemical exchange rate, whereas the increase in chemical exchange rate in Figure 4.c pulls the fitted diffusive rate to slightly higher frequency. The chemical exchange portion of the curve is accurate to within 8% of the simulated value across the range of simulated noise, and the diffusive value is accurate within 40% over the same range.

Experimental Results

NMR experiments on different size and density beads were performed to verify that $T_{1\rho}$ decay was predominantly monoexponential, implying fast chemical and diffusive exchange. All large diameter beads (> 120 μm) displayed multi-exponential behavior at 25C and were excluded from further analysis. The smaller diameter beads (50 μm) displayed predominantly mono-exponential behavior at 25C.

Further experiments on latex and Sephadex beads of similar, small sizes were made to determine if their $R_{1\rho}$ dispersion profiles displayed obvious signs of multiple frequency components. Figure 5.a shows the G25–50 bead $R_{1\rho}$ dispersion plotted with the 47-μm latex bead dispersion. The second derivative of the latex dispersion resulted in only a single zero crossing at low frequency, resulting in a single frequency component at 42.1 Hz. The remaining fitted parameters are given in Table 2.

The G25–50 bead in 5.a shows an obvious double-dispersion with midpoints near 20 Hz and 400 Hz, which is attributed to diffusive and fast chemical exchange respectively. The combination of the two diffusive processes and fast chemical exchange result in a large increase in measured $R_{1\rho}$ at all SLA values. At low SLA the additional exchange processes present in the dextran bead result in an $R_{1\rho}$ value nearly 5 times that of the latex bead of similar size.

Figure 5.b shows the results of measured $R_{1\rho}$ dispersion curves for similarly sized 50-micron diameter beads with different densities. The G25–50 beads contain a greater

concentration of dextran (~40% vs. ~10%) and display a range of $R_{1\rho}$ values approximately 5× that of the G100-50 bead. Note the fitted rates for diffusive exchange are very similar and are given in Table 2.

The results of increasing both the chemical and diffusive exchange rate with temperature are plotted in Figure 6.a. For the G100-50 bead the two fitted midpoints of dispersion increase to higher frequencies by approximately 3-fold. The results of the double-dispersion fitting are given in Table 2. The effect of selectively increasing the chemical exchange rates is shown in Figure 6.b. As the pH is increased from 6 to 9, the fitted chemical exchange rate increases with pH, whereas the fitted diffusive exchange rate remains fairly constant. The fitted parameters for Figure 6.b are also given in Table 2.

DISCUSSION AND CONCLUSIONS

Diffusion and chemical exchange may be important contributors to NMR relaxation and to MR image contrast, though their relative contributions have been seldom reported in the MR literature. Hills et al. published a series of papers exploring these contrast effects on transverse relaxation with CPMG dispersion on a model system of Sephadex beads. Spin-locking techniques may also be used to explore these processes, as they are often technically much easier to implement in an imaging context. Therefore we investigated a similar model system to determine if the relative contributions of chemical and diffusive exchange in spin-locking experiments are separable and to determine their relative contributions to measured $R_{1\rho}$. The distinct exchange processes of diffusive exchange from water and hydroxyl protons within the bead to free water, of diffusion through susceptibility gradients, and of chemical exchange are depicted in Figure 1.

Numeric simulations of double dispersion data with a three-pool model of chemical exchange verified that the exchange processes of diffusion and chemical exchange result in a double-dispersion $R_{1\rho}$ profile if the two processes have sufficiently separated mean frequencies. Figure 2 depicts the effect of modulating the magnitude of the frequency step of either diffusive exchange between the interior and exterior of the Sephadex or migration of spins through susceptibility gradients. The frequency step was decreased from a high rate of the chemical shift, representing no contribution from susceptibility effects, down an order of magnitude to a rate of $0.1*\delta\omega$, representing a dephasing contribution from susceptibility effects only. The upper rate is consistent with the chemical shift of dextran and the lower rate is consistent with prior reports of the contribution of susceptibility gradients to T_2 contrast in CPMG experiments (6). Therefore, Figure 2 demonstrates the range of frequencies (midpoints of the dispersion curves) that may reasonably be expected for both types of diffusive exchange in a model system of Sephadex beads in the absence of rapid chemical exchange. The midpoint of the dispersion curve is seen to scale with chemical shift and exchange rate as expected by Chopra et al. and others (8,24). The magnitude of $R_{1\rho}$ dispersion for Figure 2.a should be considered somewhat arbitrary, as the figure is designed to demonstrate how slow diffusion through susceptibility gradients may approximate chemical exchange at a particular rate near the midpoint of the dispersion curve, and as the Bloch equations modified for exchange do not directly model susceptibility effects. Protons traversing locally induced gradients incur gradually accruing phase changes, not the instantaneous jump between two discrete frequencies used here as a simplification. The magnitude of the contribution to $R_{1\rho}$ would be expected to scale with the gradient (and thus susceptibility change) and rate of diffusion. Susceptibility contributions to relaxation are more realistically modeled with Monte Carlo or other alternate methods, and several excellent reviews have been published on these methods (1,25,26).

Figure 2.b demonstrates the expected slow diffusive contribution of protons moving from within the bead to the surrounding water layer. Here, the midpoint of the dispersion curve moves to the right near the sum of the exchange rate and chemical shift. This is also consistent with the work of Chopra et al. and Hills et al. (2,8). This slow chemical exchange process may be modeled with the Bloch equation simulations as the theory and physical processes are more closely related (27). Figure 2.b shows that only a slight contribution of 0.1 s^{-1} is expected at the simulated rates and chemical shift.

Figure 3 demonstrates the extremes of dispersion midpoints that may be expected from rapid chemical exchange of hydroxyl protons in combination with slow diffusive exchange (3,28,29) at two field strengths. Increasing the diffusive exchange rate in Figure 3.a, results in an increased simulated $R_{1\rho}$ of ~0.2 s^{-1} at 200 MHz main field strength. There is some variation in fitted $R_{1\rho}$ values at locking fields < 30 Hz as the line width of the exchanging species is now greater than the locking field. At these extremely low locking fields, oscillations in the measured signal from off-resonance spin locking is represented in the figure as increased fitting error. Figure 3.b shows the $R_{1\rho}$ dispersion curve move to relatively higher frequency as expected as the separation between the chemical and diffusive rates is now significantly greater and is consistent with the observations of Hills (4).

Figure 4 shows the results of iteratively fitting the simulated data to the Chopra model. The key feature to observe when selecting the range of frequencies to allocate to each process is the second derivative of the double-dispersion curve. The three resulting zero-crossings correspond specifically to the inflection point of the diffusion component, the transition point between the two processes, and the inflection point of the chemical exchange component. Using the second derivative to separate each regime results in stable fittings for both chemical and diffusive exchange as long as the SNR remains above 20:1 as shown in Table 1. The chemical exchange portion of the curve is accurate to within 8% of the simulated value across the range of simulated noise, while the diffusive value is accurate only within 40% over the same range. Thus the technique is potentially more sensitive to changes in the chemical exchange portion of the double-dispersion curve than the diffusive exchange region. However, given that the expected values for the diffusion portion of the curve are on the order of 5 to 10 Hz, the fitting of these values within a range of a few Hz is potentially very useful. Figure 4.b shows that an order of magnitude change in the diffusive exchange rate is observable in the simulated and fitted results, with little observed change in the fitted chemical exchange rate. The same is not true for the fitting to simulated data in Figure 4.c, which shows the fitted diffusive exchange rate moving to higher frequency (~3 to ~18 Hz) when the simulated exchange rate is increased by an order of magnitude.

Figure 5.a shows a comparison of the effects of a latex bead of similar diameter compared to the G25–50 bead. Only a single dispersion is noted in the latex bead data, indicating the lack of a chemical exchange component. The second derivative is consistent with this observation, showing only a single zero crossing at a lower frequency. For close packed beads of radius r the gradient field will vary with spatial frequency approximately π/r. We anticipate from Eq. 3 that significant dispersion will occur around a locking frequency $\pi^2 D/r$. For a bead of diameter of 47 μm and diffusion rate D of $2.5*10^{-5}$ cm^2/s this is around 45 Hz, very close to our measured value. The observed $R_{1\rho}$ dispersion for latex is hypothesized to be from susceptibility induced dephasing alone. Knowing the change in observed $R_{1\rho}$, G_{avg} can be estimated in the solution and the $\Delta\chi$ using Eqs. 3 and 1 respectively. Using Eq. 3, if $\Delta R_{1\rho}$ is ~3.5 Hz, D is ~$2.5*10^{-9}$ m^2/s, $\gamma B_1/2\pi$ is 10 Hz and q^2D = ~42 Hz, then G_{avg} is approximately 10.5 mT/m. Using this value we estimate $\Delta\chi$ for a spherical geometry with radius 23 μm, at 9.4T, to be 0.11 ppm or 44 Hz at 400MHz B_0. This estimate is roughly 4.6 times the 0.023 ppm or 9.2 Hz $\Delta\chi$-induced dephasing component Hills et al. estimated for 50 micron Sephadex beads (4), which is consistent with the simulation in Fig. 2.a.

Figure 5.b shows the $R_{1\rho}$ dispersion data for the two 50 μm diameter Sephadex beads studied. The $R^0_{1\rho}$ value for the G100-50 bead, dextran density of roughly ~10 % (wt/wt), is 6.1 s^{-1}. The $R^0_{1\rho}$ value for the G25–50 bead, roughly 40% (wt/wt) dextran, is 23.9 s^{-1}. These values are consistent with CPMG dispersion data by Hills et al. who gave R_2 values of ~5 and 25 s^{-1} respectively (6). It's notable that the fitted diffusive and chemical exchange rates are within the same order of magnitude of each other, given the large difference in bead density. Also note that the fitted $R_{1\rho}$ rates became less precise at low SLA as is reflected in the larger error bars (1 SD). This is most likely due to inefficient locking at low rates as was noted in the simulation data. The line width of the high-density bead was ~35 Hz and so it may be expected that the applied B_1 field would fail to lock magnetization in the transverse plane below this frequency, resulting in oscillations.

Both chemical and diffusive exchange rates are expected to be sensitive to temperature, with hydroxyl chemical exchange rates expected to increase by a factor of 2.5 per 10 degrees C as predicted by Englander et al. (27). For the 15-degree rise induced, an expected increase in hydroxyl exchange rates of 3.7 times is expected. Both fitted exchange rates increased by a factor of nearly three, consistent with these predictions. The fitted $R_{1\rho}$ value at low SLA increased from a value of 6.1 s^{-1} to 10.2 s^{-1} while at high locking field, little change was noted. Both samples were tested with a starting pH of 7.4, and no correction for temperature-induced pH change was attempted, as its effect was assumed to be small as compared to the doubling of the temperature. The fitted rates are given in Table 2 and the double-dispersion plots are shown in Figure 6.a.

Figure 6.b shows the results of selectively modulating the rapid chemical exchange rate by altering the pH of the sample. The pH 6 sample had a $R^0_{1\rho}$ value of 6 s^{-1} and dropped to 0.5 s^{-1} at high SLA. The pH 7.4 sample showed much greater $R_{1\rho}$ dispersion at low frequencies, with a $R^0_{1\rho}$ value of 9 s^{-1}. The pH 9 sample showed a decreased $R^0_{1\rho}$ of 6.8 s^{-1}, however the chemical exchange inflection point moved to significantly higher frequencies, consistent with a large increase in chemical exchange rate. These chemical exchange trends are also reflected in Table 2, where the fitted chemical exchange rate increases by a factor of six. Interestingly, the fitted diffusive exchange rate remains relatively constant near 15 Hz, consistent with the simulations in Figure 3. The increase and subsequent decrease in measured $R_{1\rho}$ as the chemical exchange rate rises is consistent with simulations and may be explained by referring to Eq. 7, an analytic expression of $R_{1\rho}$ dispersion, which is a simplification of the Bloch equations given certain assumptions (8,30). The expression for $R_{1\rho}$ dispersion as derived by Chopra et al. may be simplified under the reasonable conditions of $R_{1b} < R_{2b} << r_b$ as:

$$R_{1\rho,\mathrm{obs}} \cong R_{2,A} + P_B R_{2B}\left[1 + \frac{\frac{r_B}{R_{2B}} * \Delta\omega_B^2}{r_B^2 + \Delta\omega_B^2 + \omega_1^2}\right] \quad [7]$$

where P_b is the size of the B pool, $\Delta\omega_b$ is the chemical shift, r_b is the exchange rate from pool B to A, and ω_1 is the locking field amplitude. As r_b becomes extremely high, the second term in brackets approaches zero and $R_{1\rho,\mathrm{obs}}$ decreases and becomes exchange insensitive. However, these rates are typically outside the range of physiologic relevance (28). This effect has also been recently demonstrated by Jin et al. in sugar solutions (31).

The most significant limitation of this experiment is the departure from mono-exponential decay observed at low locking field. As the locking field strength drops below the sample line width, spin locking begins to fail. This is mitigated by the use of a B_0 and B_1 compensating SL pulse (21), but as shown experimentally, the $T_{1\rho}$ fits demonstrate more

uncertainty at low SLA. This is reflected in the 1-SD error bars used in Figs. 5 and 6, and contributes to the increased size of the confidence intervals shown for both the simulated and experimental data. However, the technique appears to be sensitive enough to show trends with a controlled set of experiments. It may be more efficient and accurate to stop acquiring data when $T_{1\rho}$ fitting drops below some set R^2 value and extrapolate a fit line to lower locking field frequencies.

An additional source of error may arise from sample heating due to long duration, high power locking pulses. Data were first acquired at low power and short duration locking fields to minimize sample heating. High power, long duration pulses were acquired at the end of the experiment. Any significant sample heating would presumably increase diffusion and thus increase relaxation rates measured at high power. As figures 5 and 6 asymptotically approach a minimum value near ~10 kHz, any heating effect is thought to be minimal.

It would be interesting to compare the simulation and experimental results from the Bloch-McConnel equations to similar parameters using the finite element or Monte Carlo methods required for the Bloch-Torrey equations. Additionally, it may be more efficient to fit these double-dispersion data in one step with Halle's model-free analysis techniques for multiple dispersion curves, rather than the iterative approach used here (32).

In conclusion, we have demonstrated that combined chemical and fast diffusive exchange may be approximated as a fast and slow chemical exchanging component in $R_{1\rho}$ dispersion curves with simulations and experiments on a simple system of Sephadex beads. The resulting double-dispersion curves may be fit with an extension of Chopra's chemical exchange model. These data may be of use for investigating systems where diffusion effects are an important contributor to relaxation.

Acknowledgments

NCRR 1S10 RR17799

NIH R01 EB000214

APPENDIX

This notation corresponds to a three-pool system of free water A and exchange processes due to chemical exchange in pool B and diffusive exchange in pool C. Variations in the rates of k and κ are used to modulate exchange among pools.

$$\mathbf{M}_i = \mathbf{A} - \mathbf{M} + \mathbf{M}', \quad [1]$$

where

$$M = \begin{bmatrix} M_a \\ M_b \\ M_c \end{bmatrix} \text{ and } \mathbf{M}_i = \begin{bmatrix} M_x^i \\ M_y^i \\ M_z^i \end{bmatrix}, \text{ i=a, b, c}$$

and A is the 9 × 9 matrix

$$A=\begin{bmatrix} a & \prod(k_b+\kappa_b) & \prod\kappa'_{-c} \\ \prod(k_a+\kappa_a) & b & \prod\kappa_{-c} \\ \prod\kappa'_c & \prod\kappa_c & c \end{bmatrix} \quad [2]$$

where Π is the 3 × 3 identity matrix and

$$a=\begin{bmatrix} -(R_{2a}+k_a+\kappa_a+\kappa'_c) & (\omega-\omega_a) & \omega_1 \\ -(\omega-\omega_a) & -(R_{2a}+k_a+\kappa_a+\kappa'_c) & 0 \\ -\omega_1 & 0 & -(R_{1a}+k_a+\kappa_a+\kappa'_c) \end{bmatrix} \quad [3]$$

$$b=\begin{bmatrix} -(R_{2b}+k_b+\kappa_b+\kappa'_b) & (\omega-\omega_b) & \omega_1 \\ -(\omega-\omega_b) & -(R_{2b}+k_b+\kappa_b+\kappa'_b) & 0 \\ -\omega_1 & 0 & -(R_{1b}+k_b+\kappa_b+\kappa'_b) \end{bmatrix} \quad [4]$$

$$c=\begin{bmatrix} -(R_{2c}+\kappa'_{-c}+\kappa_{-c}) & (\omega-\omega_c) & \omega_1 \\ -(\omega-\omega_c) & -(R_{2c}+\kappa'_{-c}+\kappa_{-c}) & 0 \\ -\omega_1 & 0 & -(R_{1a}+\kappa'_{-c}+\kappa_{-c}) \end{bmatrix} \quad [5]$$

$\mathbf{M}'$ is the equilibrium vector:

$$\mathbf{M}'=\begin{bmatrix} M_a^0R_{1a} \\ M_b^0R_{1b} \\ M_c^0R_{1c} \end{bmatrix} \text{ where } \mathbf{M}_i^0=\begin{bmatrix} 0 \\ 0 \\ M_z^{i0} \end{bmatrix} \quad \text{I=a, b, c} \quad [6]$$

Resonance frequency offsets may be explicitly accounted for with the following expressions:

$$\omega-\omega_a=\omega_z+(1-P_a)\delta\omega+P_c\delta\Omega, \quad [7]$$

$$\omega-\omega_b=\omega_z+P_a\delta\omega+P_c\delta\Omega, \quad [8]$$

$$\omega-\omega_c=\omega_z-P_a\delta\omega-(P_a+P_b)\delta\Omega, \quad [9]$$

where $\delta\omega = (\omega_b-\omega_a)$, $\delta\Omega = (\omega_c-\omega_b)$, and the rf offset $\omega_z = (\omega-\omega_{avg})$, where ω_{avg} is the weighted average of the resonance frequency of all three pools. Mass balance still holds in the rotating frame, so the typical flux equalities of $P_ak_a = P_bk_b$, $P_a\kappa_a = P_b\kappa_b$, $P_c\kappa'_{-c}=P_a\kappa'_c$ $P_b\kappa_c = P_c\kappa_{-c}$ and remain valid. Simulations for two-pool models may be performed by simply removing pool "C" from the model.

References

1. Kennan RP, Zhong J, Gore JC. Intravascular susceptibility contrast mechanisms in tissues. Magn Reson Med. 1994; 31(1):9–21. [PubMed: 8121277]
2. Hills, B. Magnetic resonance imaging in food science. New York: Wiley; 1998.
3. Hills BP, Babonneau F. A quantitative study of water proton relaxation in packed beds of porous particles with varying water content. Magn Reson Imaging. 1994; 12(6):909–922. [PubMed: 7526110]

4. Hills BP, Wright KM, Belton PS. Proton Nmr-Studies of Chemical and Diffusive Exchange in Carbohydrate Systems. Mol Phys. 1989; 67(6):1309–1326.
5. Meiboom S, Gill D. Modified Spin-Echo Method for Measuring Nuclear Relaxation Times. Rev Sci Instrum. 1958; 29(8):688–691.
6. Hills BP, Wright KM, Belton PS. Nmr-Studies of Water Proton Relaxation in Sephadex Bead Suspensions. Mol Phys. 1989; 67(1):193–208.
7. Hills BP, Takacs SF, Belton PS. The Effects of Proteins on the Proton Nmr Transverse Relaxation-Time of Water .2. Protein Aggregation. Mol Phys. 1989; 67(4):919–937.
8. Chopra S, Mcclung RED, Jordan RB. Rotating-Frame Relaxation Rates of Solvent Molecules in Solutions of Paramagnetic-Ions Undergoing Solvent Exchange. J Magn Reson. 1984; 59(3):361–372.
9. Hills BP, Duce SL. The influence of chemical and diffusive exchange on water proton transverse relaxation in plant tissues. Magn Reson Imaging. 1990; 8(3):321–331. [PubMed: 2164129]
10. Haacke EM, Cheng NY, House MJ, Liu Q, Neelavalli J, Ogg RJ, Khan A, Ayaz M, Kirsch W, Obenaus A. Imaging iron stores in the brain using magnetic resonance imaging. Magn Reson Imaging. 2005; 23(1):1–25. [PubMed: 15733784]
11. Zhang H, Xie Y, Ji T. Water diffusion-exchange effect on the paramagnetic relaxation enhancement in off-resonance rotating frame. J Magn Reson. 2007; 186(2):259–272. [PubMed: 17412624]
12. Beall, PT.; Amtey, SR.; Kasturi, SR. NMR data handbook for biomedical applications. New York: Pergamon Press; 1984. p. xviii198 p. p.
13. Glasel JA, Lee KH. Interpretation of Water Nuclear Magnetic-Resonance Relaxation-Times in Heterogeneous Systems. J Am Chem Soc. 1974; 96(4):970–978.
14. Woessner DE. Brownian motion and its effects in NMR chemical exchange and relaxation in liquids. Concept Magnetic Res. 1996; 8(6):397–421.
15. Harvey JM, Symons MCR, Naftalin RJ. Proton Magnetic-Resonance Study of Hydration of Glucose. Nature. 1976; 261(5559):435–436. [PubMed: 934279]
16. Hills BP. Water proton relaxation in dilute and unsaturated suspensions of non-porous particles. Magn Reson Imaging. 1994; 12(2):183–190. [PubMed: 8170295]
17. Hills BP. The Proton-Exchange Cross-Relaxation Model of Water Relaxation in Biopolymer Systems .2. The Sol and Gel States of Gelatin. Mol Phys. 1992; 76(3):509–523.
18. Woessner DE, Zhang S, Merritt ME, Sherry AD. Numerical solution of the Bloch equations provides insights into the optimum design of PARACEST agents for MRI. Magn Reson Med. 2005; 53(4):790–799. [PubMed: 15799055]
19. Molday RS, Englande Sw, Kallenrg. Primary Structure Effects on Peptide Group Hydrogen-Exchange. Biochemistry-Us. 1972; 11(2) 150-&.
20. Sepponen RE, Pohjonen JA, Sipponen JT, Tanttu JI. A method for T1 rho imaging. J Comput Assist Tomogr. 1985; 9(6):1007–1011. [PubMed: 4056129]
21. Witschey WR 2nd, Borthakur A, Elliott MA, Mellon E, Niyogi S, Wallman DJ, Wang C, Reddy R. Artifacts in T1 rho-weighted imaging: compensation for B(1) and B(0) field imperfections. J Magn Reson. 2007; 186(1):75–85. [PubMed: 17291799]
22. Regatte RR, Akella SV, Borthakur A, Reddy R. Proton spin-lock ratio imaging for quantitation of glycosaminoglycans in articular cartilage. J Magn Reson Imaging. 2003; 17(1):114–121. [PubMed: 12500280]
23. Cobb JG, Xie J, Gore JC. Contributions of chemical exchange to T1ρ dispersion in a tissue model. Magnet Reson Med. 2011 n/a-n/a.
24. Cobb JG, Xie J, Gore JC. Contributions of chemical exchange to T1ρ dispersion in a tissue model. Magnet Reson Med. 2011 [Epub ahead of release].
25. Hardy P, Henkelman RM. On the Transverse relaxation rate enhancement induced by diffusion of spins through inhomogeneous fields. Magnet Reson Med. 1991; 17(2):348–356.
26. Pathak AP, Ward BD, Schmainda KM. A novel technique for modeling susceptibility-based contrast mechanisms for arbitrary microvascular geometries: The finite perturber method. Neuroimage. 2008; 40(3):1130–1143. [PubMed: 18308587]

27. Englander SW, Downer NW, Teitelbaum H. Hydrogen exchange. Annu Rev Biochem. 1972; 41:903–924. [PubMed: 4563445]

28. Liepinsh E, Otting G. Proton exchange rates from amino acid side chains - Implications for image contrast. Magnet Reson Med. 1996; 35(1):30–42.

29. Hills BP, Cano C, Belton PS. Proton Nmr Relaxation Studies of Aqueous Polysaccharide Systems. Macromolecules. 1991; 24(10):2944–2950.

30. Trott O, Palmer AG 3rd. R1rho relaxation outside of the fast-exchange limit. J Magn Reson. 2002; 154(1):157–160. [PubMed: 11820837]

31. Jin T, Autio J, Obata T, Kim S-G. Spin-locking versus chemical exchange saturation transfer MRI for investigating chemical exchange process between water and labile metabolite protons. Magnet Reson Med. 2011; 65(5):1448–1460.

32. Halle B, Johannesson H, Venu K. Model-free analysis of stretched relaxation dispersions. J Magn Reson. 1998; 135(1):1–13. [PubMed: 9799667]

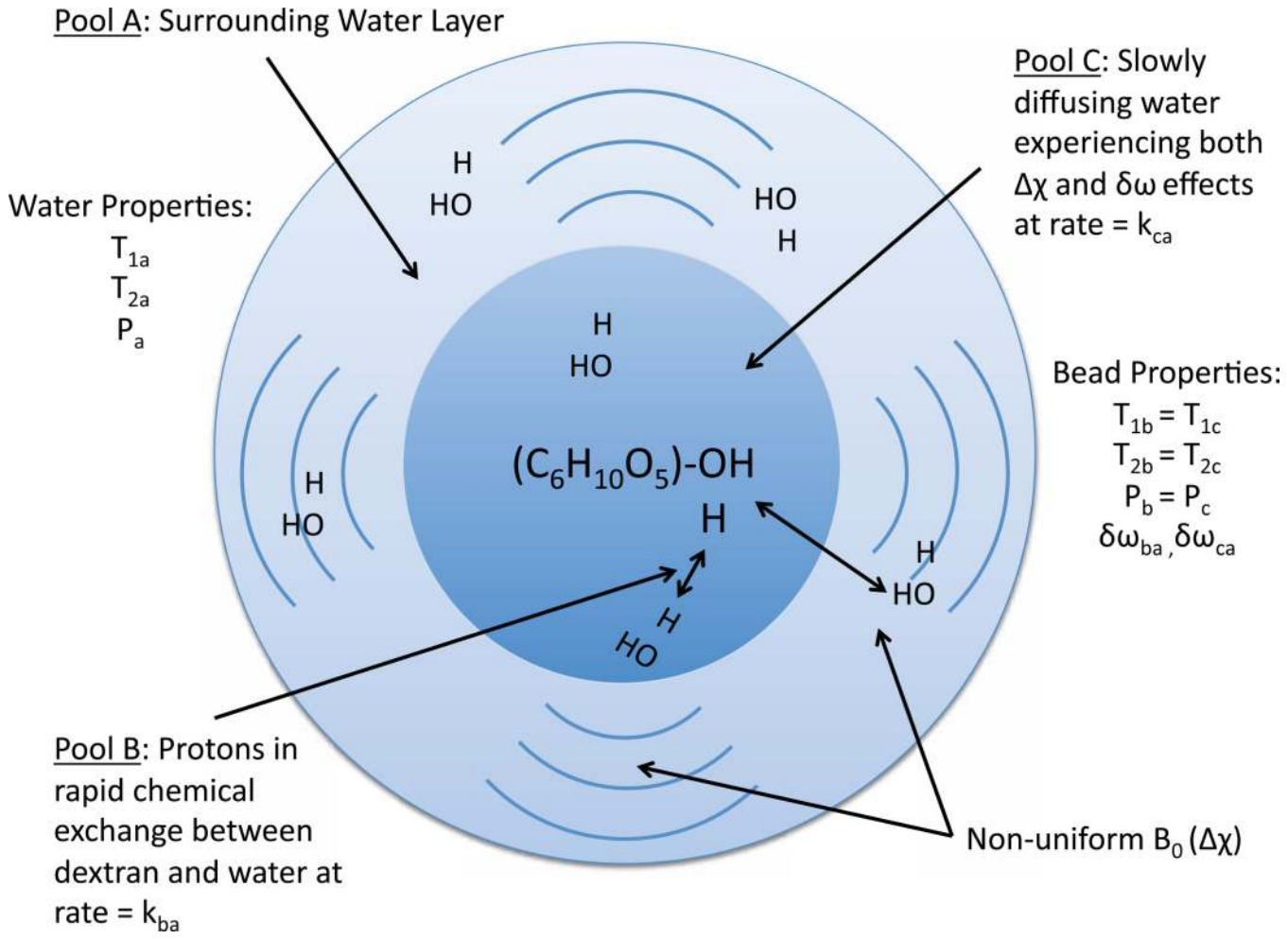

Figure 1.

A model of chemical and diffusive exchange. The Sephadex bead approximates a sphere on the order of tens of microns in radius, and is composed of cross-linked dextran with numerous $^{-}$OH exchange sites. Pool A represents free water, Pool B represents surface $^{-}$OH groups in rapid exchange with water at rate k_{ba}, Pool C represents interior $^{-}$OH groups in diffusive exchange from within the bead to the surrounding water at rate k_{ca}.

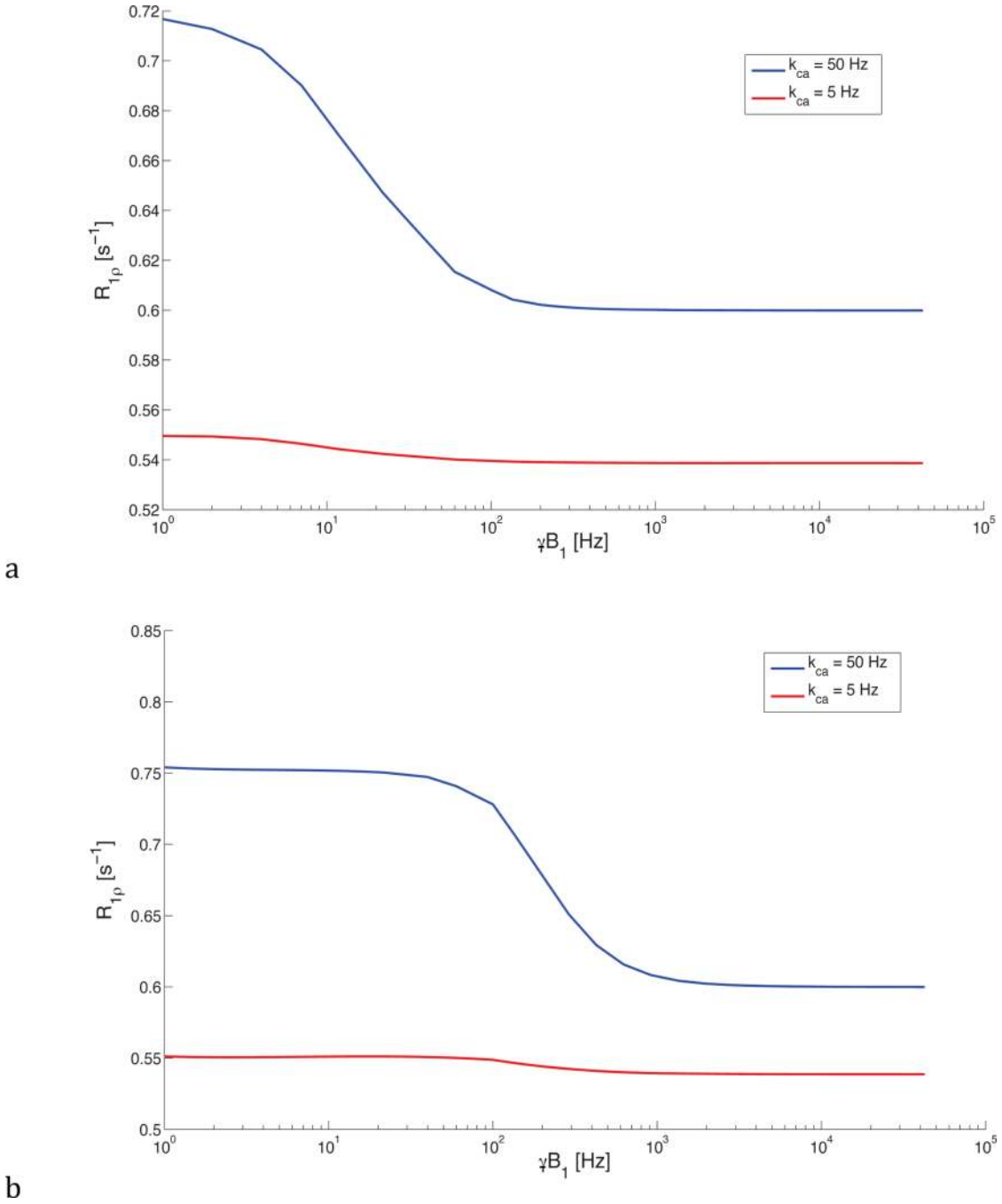

Figure 2.

Simulations estimating expected $R_{1\rho}$ relaxation due to diffusion related dephasing as spins encounter susceptibility-induced gradients with an estimated chemical shift estimated as $\delta\omega_{ca}$ = 0.123 ppm (2.a) or due to diffusion approximating slow chemical exchange with chemical shift $\delta\omega_{ca}$ = 1.23 ppm (2.b).

a. Estimated susceptibility-induced relaxation as the observed diffusion exchange rate (k_{ca}) increases from 5–50 Hz with chemical shift of $\delta\omega_{ca}$ = 0.123 ppm or ~25 Hz at 200 MHz main field. Note a single inflection point near ~25 Hz that scales with the increased exchange rate.

b. Estimated diffusion-induced relaxation observed as the slow diffusion exchange rate (k_{ca}) increases from 5–50 Hz with $\delta\omega_{ca}$ = 1.23 ppm or ~250 Hz at 200 MHz main field. Note a single inflection point near ~250 Hz that scales with the increased exchange rate.

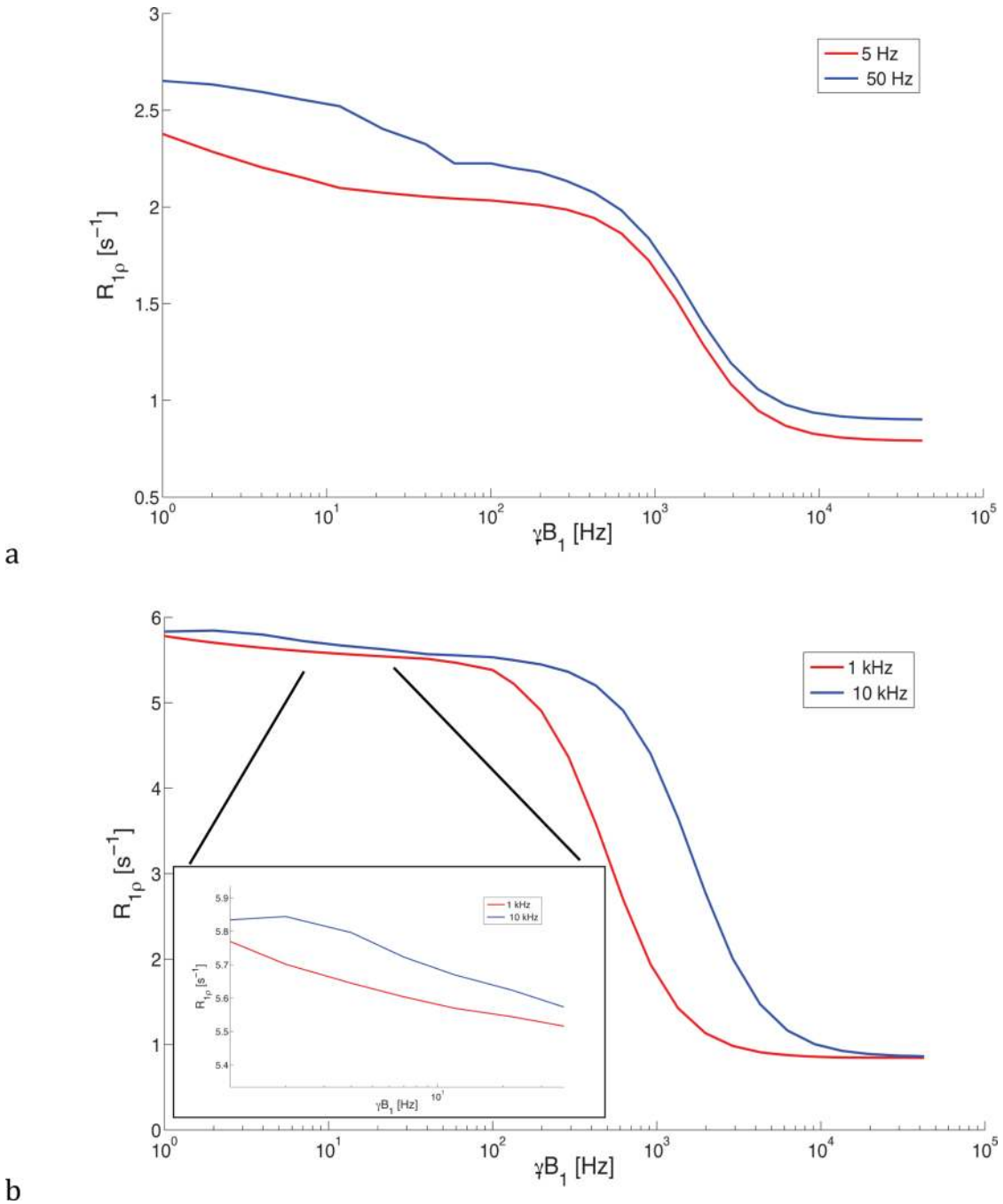

Figure 3. Simulations of chemical and diffusive exchange contributions to $R_{1\rho}$ relaxation

a. Simulation of $R_{1\rho}$ dispersion at 200 MHz with an increasing diffusive exchange rate (from 5 to 50 Hz) and a constant chemical exchange rate. Note the subtle rise in $R_{1\rho}$ dispersion at locking field < 100 Hz.

b. A Simulation of $R_{1\rho}$ dispersion at 400 MHz with an increasing chemical exchange rate (from 1 kHz to 10 kHz) and a constant diffusive exchange term of 5 Hz. Note the large increase in $R_{1\rho}$ dispersion at locking fields > 100 Hz. The inset figure shows the dispersion below 100 Hz.

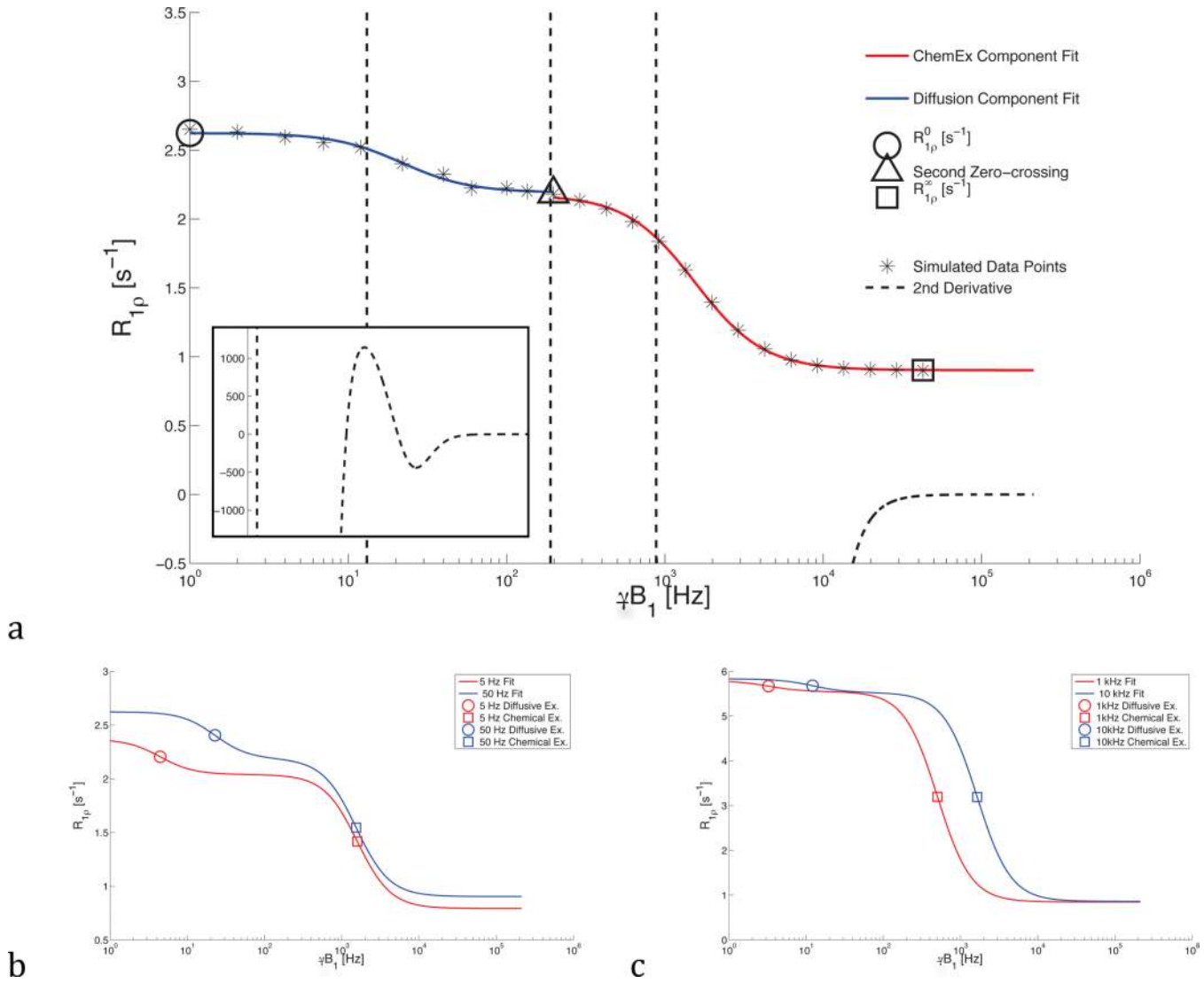

Figure 4. Chemical and Diffusive Exchange Model Fitting

a. Iterative fitting of simulated $R_{1\rho}$ double-dispersion due to chemical and diffusive exchange with the Chopra equation (Eq. 5). The second derivative of the $R_{1\rho}$ dispersion data was calculated and the second zero crossing used to identify the inflection point between the chemical and diffusive exchange regimes (~200 Hz). The full second derivative is plotted in the inset figure. The Chopra equation was applied in an iterative fashion between locking fields of 0 and 200 Hz, and again between 200 Hz and 10 kHz. The midpoints of the diffusive and chemical exchange portions of the curve (S_ρ in Eq. 5) are shown with a 5- and 6-pointed star respectively.

b. Fitting of simulated $R_{1\rho}$ double-dispersion curves with the iterative Chopra technique. Figure 3.b shows the fittings from a 5 Hz diffusion component increasing to 50 Hz with a chemical exchange rate of 10 kHz. Note that the mid-point of the chemical exchange region of the curve (S_ρ) remains relatively constant with increased diffusion.

c. Shows the fittings from a simulation of a 5 Hz diffusion component and a chemical exchange rate that increases from 1 kHz to 10 kHz. Note that the increase in chemical exchange rate also increases the fitted diffusion component.

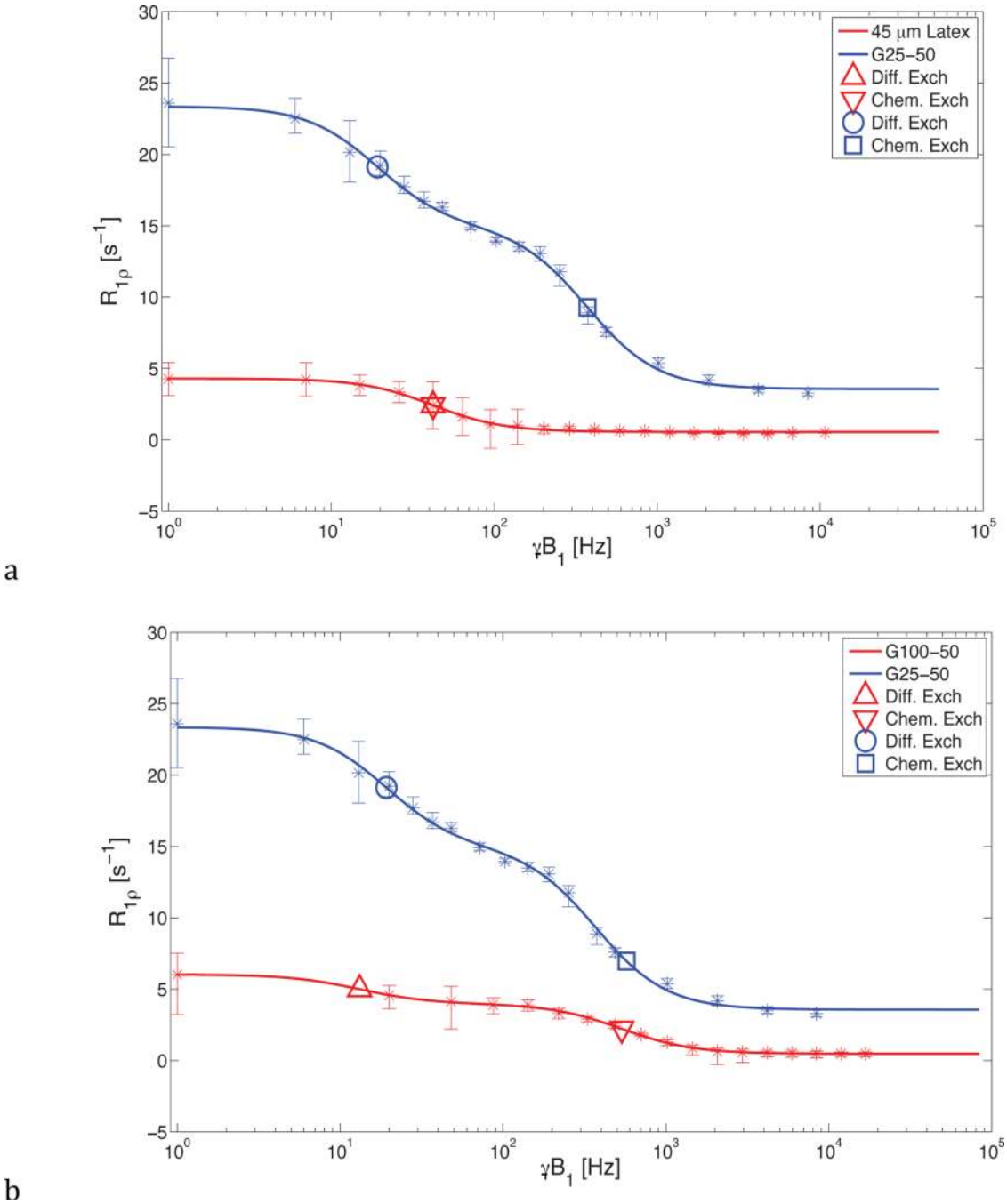

Figure 5. Sephadex and Latex Bead Dispersion Experiments

a. The G-25 bead shows a double-dispersion profile, characteristic of chemical and diffusive, and/or susceptibility-induced exchange. The latex bead's second derivative only contains one zero transition at low frequency, indicating a lack of a chemically exchanging species.

b. Figure 5.b shows the characteristic double dispersion curves for the G25–50 and G100-50 beads. The increased density of the G25–50 bead results in an increase in $R_{1\rho}$ values across the entire range of locking field frequencies. The iterative fits to the Chopra equation (Eq. 5) are shown along with the mid-points (S_ρ) for both chemical and diffusive exchange.

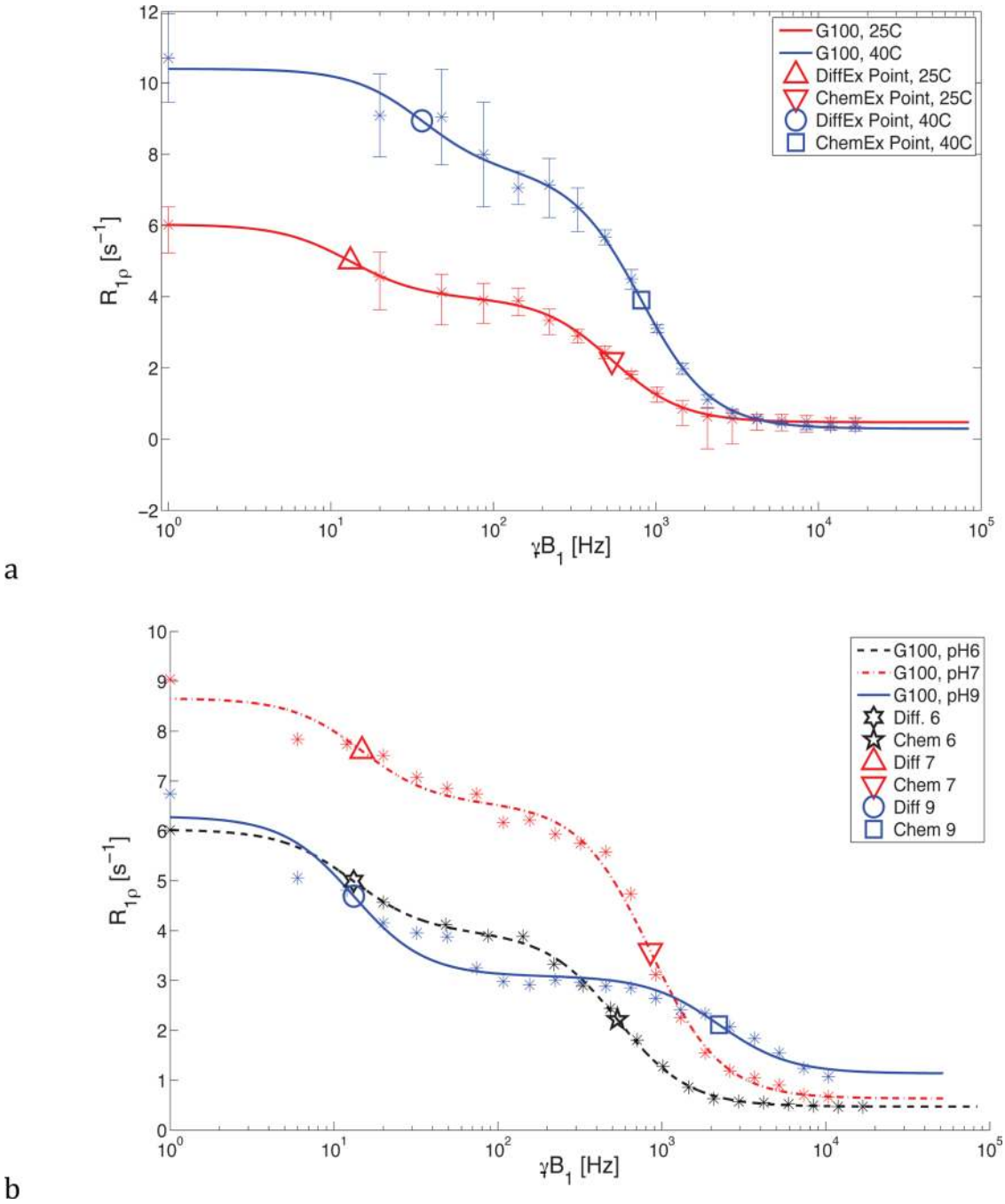

Figure 6. Figure 6 shows the sensitivity of chemical and diffusive exchange rates to changes in temperature and pH

a. $R_{1\rho}$ dispersion profiles for G100-50 at 25 and 40 deg. C. Note that both the chemical and diffusive rates are sensitive to temperature perturbation as expected.

b. $R_{1\rho}$ dispersion profiles for G100-50 at pH 6,7, and 9. Note that the fitted mid-point (S_ρ) for chemical exchange rate increases with increasing pH, while the diffusive exchange term remains fairly constant.

Table 1

Fitting Methods Compared

		SNR = 100:1	80	60	40	20	10
Chopra Fits	ChemEx	960.2 (± 17)	969.7 (± 21)	1054.5 (± 38)	924.7 (± 82)	806.6 (± 61)	829.2 (± 370)
	DiffEx	3.0 (± 2.7)	3.5 (± 2.8)	4.0 (± 5.8)	6.3 (± 5.5)	5.3 (±8.3)	n/a
		SNR = 100:1	80	60	40	20	10
% Variance	ChemEx	3.98%	3.03%	5.45%	7.53%	19.34%	17.08%
	DiffEx	39.40%	29.82%	19.13%	26.03%	5.66%	n/a

Magn Reson Med. Author manuscript; available in PMC 2014 May 01.

Table 2

Fitted Data from Figures 5 and 6

Fig. 5.a.	Substance	Diffusive Exch. Rate [Hz]	Chemical Exch. Rate [Hz]
	47 μM Latex	42.1 (± 1.8)	n/a
	G25–50	19.2 (± 1.9)	2270 (± 520)
Fig. 5.b.	Substance	Diffusive Exch. Rate [Hz]	Chemical Exch. Rate [Hz]
	G100-50	13.2 (± 1.4)	1393 (± 330)
	G25–50	19.2 (± 1.9)	2270 (± 520)
Fig. 6.a.	Substance	Diffusive Exch. Rate [Hz]	Chemical Exch. Rate [Hz]
	G100-50 25C	13.2 (± 1.4)	1393 (± 330)
	40C	36.3 (± 9.0)	4140 (± 136)
Fig. 6.b.	Substance	Diffusive Exch. Rate [Hz]	Chemical Exch. Rate [Hz]
	G100 pH6	13.2 (± 1.4)	1365 (± 280)
	pH7	13.1 (± 1.4)	4596 (± 404)
	pH9	14.8 (± 1.4)	8650 (± 2385)